ARRAY OF MESOSCOPIC ENSEMBLES ON A MAGNETIC ATOM CHIP

A. F. TAUSCHINSKY, C. F. OCKELOEN, R. M. T. THIJSSEN,
S. WHITLOCK and R. J. C. SPREEUW*

Van der Waals-Zeeman Institute, University of Amsterdam,
Valckenierstraat 65, 1018 XE Amsterdam, the Netherlands
**E-mail: r.j.c.spreeuw@uva.nl*
www.science.uva.nl/research/aplp/

We report on the storage and manipulation of hundreds of mesoscopic ensembles of ultracold ^{87}Rb atoms in a vast two-dimensional array of magnetic microtraps, defined lithographically in a permanently magnetized film. The atom numbers typically range from tens to hundreds of atoms per site. The traps are optically resolved using absorption imaging and individually addressed using a focused probe laser. We shift the entire array, without heating, along the surface by rotating an external bias field. We evaporatively cool the atoms to the critical temperature for quantum degeneracy. At the lowest temperatures, density dependent loss allows small and well defined numbers of atoms to be prepared in each microtrap. This microtrap array is a promising novel platform for quantum information processing, where hyperfine ground states act as qubit states, and Rydberg excitation may orchestrate interaction between neighbouring sites.

Keywords: atom chip; neutral atoms; mesoscopic ensembles; quantum information; lattice; microtrap.

1. Introduction

We are investigating a unique experimental system combining trapped neutral atoms which offer precise quantum control, with solid-state-like technology to create a novel platform for quantum information science. Our atom chip consists of a lithographically defined pattern of permanently magnetized film, which creates a vast two-dimensional array of magnetic microtraps.[1] This approach benefits from modern hard-disk technology making it possible to scale cold-atom experiments to thousands of samples in nearly arbitrary configurations. Additionally, arrays of small atomic ensembles can be prepared while maintaining optically resolvable separations to allow in-

dividual control over internal quantum states. Previous work has employed one-dimensional magnetic arrays using periodically magnetized videotape[2] and grooved TbGdFeCo films.[3] This experiment is the first to employ a two-dimensional configuration.[4]

2. Experimental results

2.1. *Magnetic-film atom chip*

At the core of our experiment is a magnetic chip, consisting of a 300-nm thick FePt film (Hitachi) on a silicon substrate, patterned using optical lithography into a two-dimensional lattice, see Fig. 1(a). The lattice periods are 22 μm and 36 μm corresponding to 1250 traps/mm^2. The film is permanently magnetized out-of-plane in a 5 T field. The field produced near the surface is equivalent to an effective edge current of 0.2 A along the

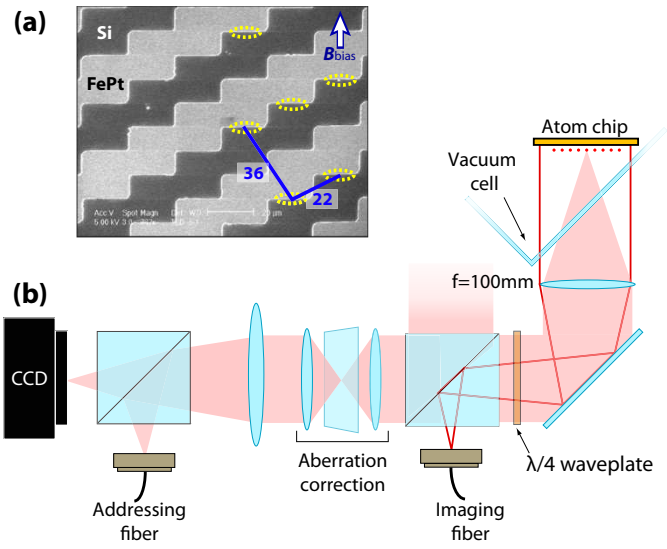

Fig. 1. (a) SEM picture of the patterned magnetic-film atom chip, showing the magnetic FePt film in light grey, the silicon substrate in dark grey. For the experiment, the chip was coated by a reflective gold coating. A 20 G bias field (arrow) yields magnetic field minima (dashed ellipses) at 10 μm distance from the surface. The lattice parameters are 22 μm and 36 μm. (b) Optics for reflective absorption imaging and individual addressing. Weak resonant probe light from the "imaging fiber" is collimated on the chip surface. The probe light is reflected by the chip and then imaged onto the CCD camera. Light from the "addressing fiber" can be focused on an individual lattice site for local manipulation.

borders of the pattern. If realized using gold microwires it would require a power dissipation of 30 W/mm^2, highlighting the advantage of permanent magnets over conductors for large scale integration of magnetic microtraps. To produce the traps, a uniform external field of 20 G is superimposed, producing an array of magnetic minima positioned 10 μm above the surface. For this bias field the trap frequencies are 6.1 kHz and 15 kHz and the trap depth, defined as the barrier between nearest neighbours, is 500 μK.

2.2. *Imaging and optical addressing*

The array of microtraps is loaded by merging the field of a macroscopic Z-wire trap containing atoms with that of the lattice. After transfer the Z-wire current is switched off. Resonant reflection absorption imaging, see Fig. 1(b) is then used to provide a two-dimensional view of the atomic distribution. Shown in Fig. 2(a) is a typical absorption image (in false color) obtained by dividing a raw probe image with an optimized reference image to obtain the fringe-free optical density distribution. The optical resolution (5 μm) is slightly improved as compared with Ref. 1 through the addition of a tilted glass plate in the imaging path (Fig. 1(b)) to compensate distortion due to the vacuum cell. Each spot (optical resolution 5 μm) corresponds to a single trap containing approximately 500 atoms. In total there are more than 500 populated microtraps.

In addition to imaging the atoms our setup is used to locally manipulate

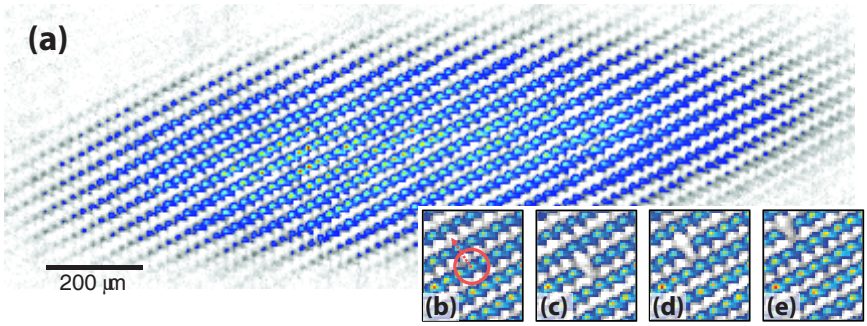

Fig. 2. (a) Typical absorption image of the magnetic lattice, with approximately 500 sites filled with typically 500 atoms per site in the center. The inset (b), shows the position of the focused optical pumping "addressing" laser targeting a single site (circled). (c) Emptied site after pulsing on the addressing laser. (d,e) The entire lattice, including the empty site, was then transported along the surface by rotating the external bias field, over up to five lattice periods (two shown) and back, in 18 ms per lattice period.

atoms using focused lasers. An addressing beam from the output of a single mode optical fiber is positioned within a secondary imaging plane created by a beam-splitter placed in front of the CCD camera, see Fig. 1(b). The beam is then effectively imaged to the chip surface (demagnification factor of 3) where it is aligned with a single array site near the center of the distribution (Fig. 2(b)). The laser is stabilized to the $F = 2 \rightarrow F' = 3$ optical pumping transition which has a high probability of flipping the spin of the atoms to an untrapped magnetic state. The laser is pulsed on for 1 ms, rapidly emptying the trap (Fig. 2(c)). Importantly, the neighbouring traps are unaffected by this pulse indicating negligible cross-talk. In the future, this probe may be replaced by a spatial light modulator to address multiple traps in sequence or in parallel.

2.3. *Shift register*

Additional parallel operations on the array are possible using uniform external fields. We have realized an atomic shift register — the analog of an electronic CCD — which is a key ingredient for quantum information processing with neutral atoms. By rotating the external bias magnetic field it is possible to transport the atom clouds in parallel across the chip surface, see Fig. 2(b–d). A field sequence optimized for a constant trap height of 10 μm and smooth transport (trap bottom of 3.23 G), is applied via three pairs of external Helmholtz coils at a rate of 18 ms per shift period. This sequence is repeated up to five times and then reversed for five times to shift back to the original position with a round trip distance of 360 μm. No additional heating is observed during transport.

2.4. *Approaching quantum degeneracy*

Efficient evaporative cooling of the atom clouds is performed using a 280-ms duration radio frequency sweep. Using absorption imaging and radio frequency spectroscopy we determine the number of atoms and temperature of each individual cloud in the array. As shown in Fig. 3 the temperature distribution across the lattice begins rather uniform at around 50 μK (presumably limited by the finite trap depths). The rf sweep rapidly reduces the mean temperature, and at temperatures below 5 μK, density dependent loss due to three-body recombination plays a strong role, see Fig. 4. The phase-space distribution at low temperatures approaches a constant phase space density as indicated by the solid line in Fig. 3 which is the calculated critical density for Bose–Einstein condensation including finite size effects and

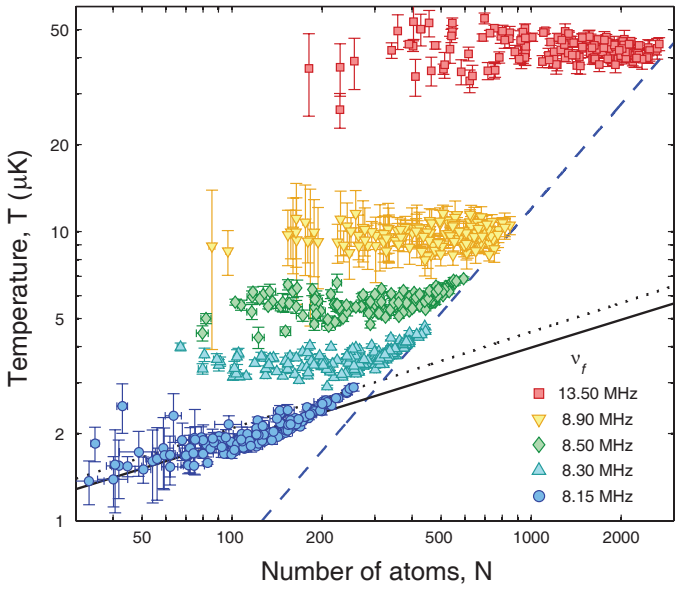

Fig. 3. Temperature vs. atom number in individual traps after radio-frequency evaporative cooling. Each data point represents an individual lattice site. Different symbols correspond to evaporation runs with different trap depth as determined by the final frequency of the "rf knife". Initially all clouds have approximately the same temperature. For the lowest trap depth the distribution clusters at a constant phase space density ~ 2.612 (solid line), due to strong density-dependent losses. Approximately 50% of sites are in the quantum degenerate regime, with condensate fractions of $\sim 10\%$.

interactions. At the lowest trap depths the distribution is consistent with $\sim 50\%$ of sites partially degenerate (condensate fraction $\sim 10\%$). Lower temperatures and higher condensate fractions could be achieved using the $|F = 1, m_F = -1\rangle$ hyperfine state of ^{87}Rb which has a lower three-body rate coefficient. Our interest however is in the single atom regime, therefore, we have investigated density dependent loss as a mechanism to prepare small and well defined number of atoms in each trap.

For the lowest measured temperatures, clouds of atoms are produced containing below 50 atoms/site, and smaller clouds are obtained via three-body recombination losses. This places our system in an interesting regime, namely between individual microtraps on atom chips, which may contain 10^3–10^4 atoms and the microscopic regime of optical lattices which typically contain 1 atom per site. However, we maintain individually resolvable microtraps and benefit from having many traps in parallel. Our experiments

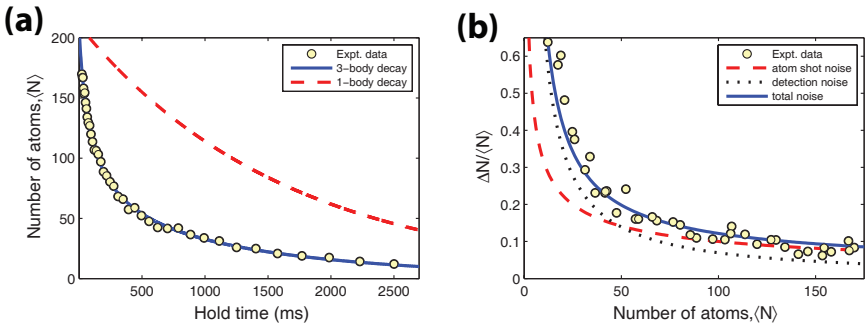

Fig. 4. (a) Decay of the atom number in a single site in the lattice. The decay is strongly non-exponential as a result of three-body recombination. (b) Atom number fluctuations for one selected site in the lattice. The mean atom number $\langle N \rangle$ and the standard deviation ΔN were obtained from 40 absorption images. The dashed line shows the expected atom shot noise, the dotted line the detection noise. The solid line combines these two noise sources. Atom shot noise dominates for $\langle N \rangle > 50$.

range from a few atoms to more than 100 atoms per microtrap allowing unique access to many-body physics and quantum fluctuations.

2.5. *Mesoscopic ensembles and atom number fluctuations*

To analyse the fluctuations of atom number intrinsic to mesoscopic ensembles we measure the number of atoms in a single site. The integrated atom number for a selected site was determined by least-squares fitting the cropped images with a two-dimensional Gaussian profile, with a fixed position, width, and orientation as determined by the observed optical density distribution. By varying the hold time in the trap between 0 and 2.50 s with an rf knife at a fixed frequency of $\nu_f = 8.30$ MHz ($T \sim 4$ μK), we observe rapid non-exponential loss of atoms due to three-body recombination. The experiment is repeated 38 times for each of 40 different hold times (1520 images in total). In Fig. 4(a) we show the mean number of atoms in the trap $\langle N \rangle$ measured as a function of hold time t. The measured atom number ranges from 170 atoms for $t = 23$ ms down to 12 atoms for $t = 2500$ s. To the data we fit a simple model which describes loss of atoms including three-body decay and one-body (background collisional) loss.

$$\langle N(t) \rangle = \frac{N(0)\, e^{-t/\tau}}{\sqrt{1 + \gamma\tau(1 - e^{-2t/\tau})}} \tag{1}$$

where $N(0)$ is the initial number of atoms in the trap, τ is the one body decay time constant, and γ is the three-body decay rate proportional to

the mean squared density in the trap. From the fit we find $N(0) = 210 \pm 4$, $\gamma = 9.7 \pm 0.7$ s^{-1} and $\tau = 1.6 \pm 0.2$ s. For short hold times, the loss is strongly density dependent, with a three-body loss rate 15 times larger than the one-body loss rate.

In addition to the average number of atoms in the trap we also determine the atom number fluctuations. Shown in Figure 4(b), are the relative fluctuations $\Delta N/\langle N\rangle$ as a function of the mean atom number. We find that the relative fluctuations grow rapidly with decreasing atom number. Shown in Fig. 4 are the expected fluctuations due to poissonian noise (atom shot noise) which has a $1/\sqrt{N}$ dependence and a estimated detection noise, based on the residual pixel noise and the size of the atomic distribution (determined by the point-spread-function), which scales with $1/N$ (ΔN=constant). We observe good agreement of the data with the combination of these two noise sources with no free parameters. For $N > 50$ atoms, atomic shot noise dominates the observed fluctuations, while below this number, detection noise plays a significant role. The estimated detection noise limit for these images (corresponding to a signal-to-noise ratio of 1) is 7 atoms/trap/shot.

In the future we plan to further improve our detection sensitivity to reach the single-atom regime, for example by increasing the numerical aperture of the imaging optics. Our analysis of trapped few-atom ensembles can also be extended over the full lattice through *in-situ* spatial correlation analysis.

3. Outlook

Our envisioned scheme for quantum information processing in this system involves writing hyperfine state coherence into individual traps, storing quantum information either in single atoms, or as collective hyperfine excitations in mesoscopic ensembles.[5,6] As a first step we have observed Ramsey interference using microwave+rf two-photon coupling, driving the two-photon transition between the prospective qubit states, $|0\rangle = |F = 1, m_F = -1\rangle \leftrightarrow |1\rangle = |F = 2, m_F = 1\rangle$, see Fig. 5. The fringe contrast of $\sim$80% is consistent with a $\sim$100 ms coherence time.

Interactions between qubits in different sites can be controlled using long-range interactions between Rydberg atoms. The key effect, the Rydberg dipole blockade has recently been demonstrated for distances up to 11 μm.[7,8] Resonant dipole-dipole interaction has even been observed at distances of 40 μm.[9] In a next generation of atom chip we will aim for a lattice spacing of 5 μm, in order to facilitate the Rydberg blockade and still be

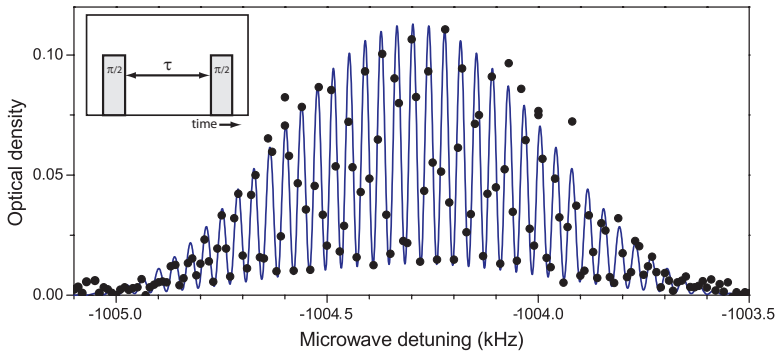

Fig. 5. Ramsey fringes in a single magnetic trap. Two $\pi/2$ pulses of combined microwaves and radio frequency waves were applied, driving the ground state hyperfine transition $|F = 1, m_F = -1\rangle \leftrightarrow |F = 2, m_F = 1\rangle$. The microwave frequency was varied; the time between the pulses was $\tau = 25$ ms.

able to optically resolve individual sites.

4. Conclusions

We have demonstrated a novel experimental systems allowing the preparation and study of hundreds of mesoscopic samples of ultracold atoms in a two-dimensional array of magnetic microtraps. The traps have been loaded, cooled, optically resolved and adddressed, and transported along the surface. This array has great potential as a novel platform for quantum information science and for studying fluctuations in mesoscopic systems.

Acknowledgments

This work is part of the research programme of the "Stichting voor Fundamenteel Onderzoek der Materie (FOM)", which is financially supported by the "Nederlandse Organisatie voor Wetenschappelijk Onderzoek (NWO)". The chips were patterned in the Amsterdam *nano*Center. SW acknowledges support from a Marie-Curie individual fellowship (grant number PIIF-GA-2008-220794).

References

1. S. Whitlock, R. Gerritsma, T. Fernholz and R. J. C. Spreeuw, *New J. Phys.* **11**, p. 023021(February 2009).
2. C. D. J. Sinclair, J. A. Retter, E. A. Curtis, B. V. Hall, I. Llorente Garcia, S. Eriksson, B. E. Sauer and E. A. Hinds, *Eur. Phys. J. D* **35**, 105 (2005).

3. M. Singh, M. Volk, A. Akulshin, A. Sidorov, R. Mclean and P. Hannaford, *J. Phys. B: At. Mol. Opt. Phys.* **41**, 065301+ (2008).
4. R. Gerritsma, S. Whitlock, T. Fernholz, H. Schlatter, J. A. Luigjes, J. U. Thiele, J. B. Goedkoop and R. J. C. Spreeuw, *Phys. Rev. A* **76**, p. 033408 (2007).
5. M. D. Lukin, M. Fleischhauer, R. Cote, L. M. Duan, D. Jaksch, J. I. Cirac and P. Zoller, *Phys. Rev. Lett.* **87**, 037901+(June 2001).
6. M. Müller, I. Lesanovsky, H. Weimer, H. P. Büchler and P. Zoller, *Phys. Rev. Lett.* **102**, p. 170502 (2009).
7. E. Urban, T. A. Johnson, T. Henage, L. Isenhower, D. D. Yavuz, T. G. Walker and M. Saffman, *Nat Phys* **5**, 110(February 2009).
8. A. Gaetan, Y. Miroshnychenko, T. Wilk, A. Chotia, M. Viteau, D. Comparat, P. Pillet, A. Browaeys and P. Grangier, *Nat Phys* **5**, 115(February 2009).
9. C. S. E. van Ditzhuijzen, A. F. Koenderink, J. V. Hernandez, F. Robicheaux, L. D. Noordam and H. B. van Linden van den Heuvell, *Phys. Rev. Lett.* **100**, p. 243201 (2008).